*Progress In Electromagnetics Research B, Vol. 58, 123–138, 2014*

# Electromagnetic Interactions Analysis between Two 3-D Scatterers Using the E-PILE Method Combined with the PO Approximation

**Mohammad Kouali[1, *], Gildas Kubické[2], and Christophe Bourlier[3]**

**Abstract**—In this paper, the electromagnetic scattering from two scatterers is analyzed from a rigorous integral formulation solved by the method of moments (MoM). G. Kubické has recently developed the E-PILE (Extended Propagation-Inside-Layer Expansion) method to calculate the scattering from an object above a rough surface for a two-dimensional problem. This method allows us to calculate separately and exactly the interactions between the object and the rough surface. The purpose of this paper is to extend the E-PILE method to a three-dimensional problem. Such a 3-D problem involves a large number of unknowns and can not be solved easily with a conventional method of moments by using a direct LU inversion. Thus to solve this issue, the E-PILE method is combined with the physical optics (PO) approximation to calculate the local interactions on both the object and the rough surface. By using this hybrid method, the requirements of memory and CPU time can be reduced significantly.

## 1. INTRODUCTION

In recent years, composite electromagnetic scattering from an object near a randomly rough surface has attracted considerable interest in the fields of radar surveillance, target identification, object tracking, and so on. Some methods have been developed for the efficient analysis of composite scattering for a two-dimensional problem (2-D) [1–9]. Other examples for a three-dimensional problem (3-D) can be found in [10–17]. However it is important for practical application to study the case of 3-D problem.

For a large 3-D problem, it is well known that the method of moments (MoM) is limited by the memory requirement, so some simplifying assumptions must be made. For example Ye et al. proposed a hybrid method combining analytic Kirchhoff Approximation (KA) and MoM to study the scattering from 3-D perfect electric target above a 2-D dielectric rough surface [10]. In [11] a half-space Green function with the rough surface interface is first derived from the KA, then the method of moments is applied to analyze the scattering for a 3-D problem. In [12] only small problems are investigated from a fast rigorous method. In [13, 14] some assumptions are made on the coupling mechanisms from the four-path model. In [15, 16] the electromagnetic scattering of a 3-D object above a 2-D rough surface is studied using the Finite-difference time-domain (FDTD) approach.

Moreover, even for a 2-D problem, several simplifying assumptions are made for a large one-dimensional rough surface, since a brute force MoM can be unusable. A parallelization of a rigorous method based on the MoM was proposed in [1]. In [2] a domain decomposition method with the finite-element method was applied. In [3] a hybrid algorithm, combining analytic KA and numerical method of moments MoM, is developed to solve the coupling electric-field integral equations (EFIE) of scattering from a perfect electric conducting (PEC) object above a randomly rough PEC surface. An efficient numerical PILE (Propagation-Inside-Layer Expansion) method for computing the field scattered by

*Received 12 January 2014, Accepted 29 January 2014, Scheduled 4 February 2014*

* Corresponding author: Mohammad Kouali (mohammad.kouali@gmail.com).

[1] Department of Electronic and Communication Engineering, Al-Quds University, Jerusalem, P. O. Box 20002, Palestine. [2] DGA, Information Superiority, CGN1 Division 35170 Bruz, France. [3] IETR Laboratory, Université de Nantes, L'UNAM Université, 44306 Nantes Cedex 03, France.

rough layers is proposed in [4]. In [5] an iterative method E-PILE (Extended Propagation-Inside-Layer Expansion) was combined with the Forward-Backward Spectral Acceleration (FBSA) to accelerate the computation of the local interactions on the large rough surface. In [6] the fast multipole method is used to accelerate the computation of the local interactions on the object.

Recently G. Kubické has developed a fast hybrid method for scattering from a large object with Dihedral effects above a large rough surface (2-D problem) [7]. For such a problem, the object is large, and the MoM with direct LU inversion can not be applied. Thus, to solve this issue, the E-PILE method is combined with the FBSA for the local interactions on the rough surface and with physical optics approximation (PO) for the local interactions on the object.

Very recently we have applied the Forward-Backward (FB) method to calculate the local interactions on the rough surface [17], we noticed that the complexity of the method is reduced but not enough for a large 3-D problem. In this paper, the E-PILE method is generalized to a 3-D problem, and then the physical optics approximation is combined with the E-PILE method to compute the local interactions on both the object and the rough surface. According to this it becomes unnecessary to calculate the inverse of the impedance matrix for both the object and the rough surface.

The paper is organized as follows. In Section 2 the E-PILE method is extended to study the scattering from a 3-D electromagnetic problem, coupling surface integral equations are also derived. In Section 3, the hybridization of E-PILE with PO approximation is detailed. In Section 4 numerical examples for different scenarios are presented to validate the method. The final section gives concluding remarks.

## 2. MATHEMATICAL FORMULATIONS OF THE E-PILE METHOD

Kubické et al. developed the E-PILE method to study the electromagnetic scattering from an object above a one-dimensional rough surface (2-D problem) [5]. In this paper, the E-PILE method is updated to study the scattering from a 3-D problem. Consequently the mathematical formulations of the E-PILE method is extended to the 3-D case.

Let us consider an incident electromagnetic (EM) plane wave that illuminates the system composed of two perfect electric conductor (PEC) scatterers (object+rough surface) as shown in Figure 1. The incident electromagnetic fields are written as

$$\mathbf{E}^i(\mathbf{R}) = \hat{\mathbf{e}}_i e^{i\mathbf{k}_i\cdot\mathbf{R}}, \quad \mathbf{H}^i(\mathbf{R}) = \frac{1}{\eta_0}\hat{\mathbf{k}}_i \times \mathbf{E}^i(\mathbf{R}), \tag{1}$$

where $\mathbf{k}_i = k_0\hat{\mathbf{k}}_i$, and $k_0$ and $\eta_0$ are respectively the wave number and wave impedance in air. Note that the harmonic time convention $e^{i\omega t}$ is assumed and suppressed throughout this paper. The plane wave in Equation (1) can be tapered to avoid edge limitations as in [12, 13].

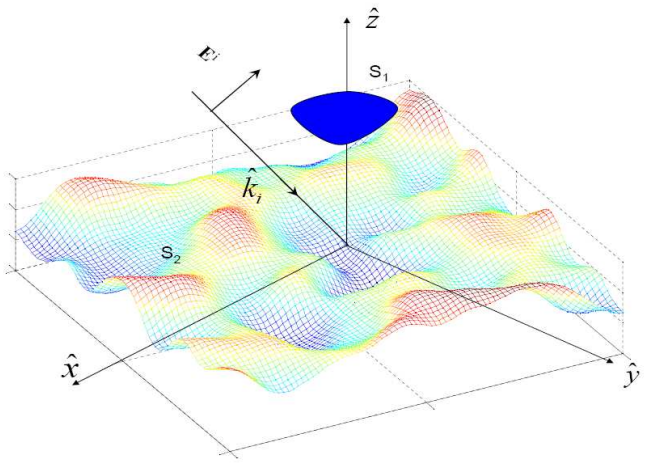


**Figure 1.** A 3-D model of an object above a rough surface.

To obtain the first coupling integral equation between $S_1$ and $S_2$ we use the boundary conditions on scatterer 1 (the object) $S_1$, $\forall\, \mathbf{R}' \in S_1$

$$\hat{\mathbf{n}}_1 \times \mathbf{H}^i(\mathbf{R}') + \underbrace{\hat{\mathbf{n}}_1 \times \oint_{S_1} \mathbf{J}_1(\mathbf{R}_1) \times \nabla_{\mathbf{R}_1} G(\mathbf{R}_1, \mathbf{R}') dS}_{\text{local interactions}} + \underbrace{\hat{\mathbf{n}}_1 \times \int_{S_2} \mathbf{J}_2(\mathbf{R}_2) \times \nabla_{\mathbf{R}_2} G(\mathbf{R}_2, \mathbf{R}') dS}_{\text{coupling interactions}} = \frac{1}{2} \mathbf{J}_1(\mathbf{R}'), \quad (2)$$

where $\oint_S dS$ is the principal value integral, $G(\mathbf{R}_1, \mathbf{R}') = \exp(-ik_0 r)/4\pi r$ is the free-space Green function with $r$ the distance between the two points $\mathbf{R}_1$ and $\mathbf{R}'$, and $\mathbf{J}_1$, $\mathbf{J}_2$ are the electric currents on the two scatterers $S_1$ and $S_2$, respectively. $G(\mathbf{R}_2, \mathbf{R}') = \exp(-ik_0 r)/4\pi r$ is the free-space Green function with $r$ the distance between the two points $\mathbf{R}_2$ and $\mathbf{R}'$.

Using the boundary conditions on scatterer 2 (the rough surface) $S_2$, the second coupling integral equation $\forall\, \mathbf{R}' \in S_2$ is obtained from

$$\hat{\mathbf{n}}_2 \times \mathbf{H}^i(\mathbf{R}') + \underbrace{\hat{\mathbf{n}}_2 \times \oint_{S_2} \mathbf{J}_2(\mathbf{R}_2) \times \nabla_{\mathbf{R}_2} G(\mathbf{R}_2, \mathbf{R}') dS}_{\text{local interactions}} + \underbrace{\hat{\mathbf{n}}_2 \times \int_{S_1} \mathbf{J}_1(\mathbf{R}_1) \times \nabla_{\mathbf{R}_1} G(\mathbf{R}_1, \mathbf{R}') dS}_{\text{coupling interactions}} = \frac{1}{2} \mathbf{J}_2(\mathbf{R}'), \quad (3)$$

The use of the method of moments with point matching and pulse basis functions leads to the following linear system

$$\bar{\mathbf{Z}} \mathbf{X} = \mathbf{b}, \quad (4)$$

where $\bar{\mathbf{Z}}$ is the impedance matrix of the total scene $(S_1 \cup S_2)$ of size $(N_1 + N_2) \times (N_1 + N_2)$. The unknown vector $\mathbf{X}$ of length $(N_1 + N_2)$ is equal to

$$\mathbf{X}^T = [\mathbf{X}_1^T \ \mathbf{X}_2^T], \quad (5)$$

where $^T$ stands for transpose operator. $\mathbf{X}_1$ of length $N_1$ contains the unknown currents $\mathbf{J}_1$ on scatterer 1 in which $\mathbf{J}(\mathbf{R}_1)$ is written here as a vectorial form. In fact, Equations (2) and (3), and related vectorial quantities $\mathbf{J}_1$, $\mathbf{J}_2$, $\mathbf{H}^i$, are in fact projected on the surfaces such that they can be written as scalar equations. Thus $\mathbf{X}_1$ contains the scalar components of $\mathbf{J}_1$ (same for all other quantities below: $\mathbf{X}_2$, $\mathbf{b}_1$,...). Nevertheless, in order to write equations in compact form, all vectorial quantities are kept in a vectorial form in the linear system of MoM: the projection on the scalar components is implicit.

$$\mathbf{X}_1^T = \Big[ \underbrace{\mathbf{J}(\mathbf{R}_1^1) \ldots \mathbf{J}(\mathbf{R}_1^{N_1})}_{\text{Scatterer 1}} \Big], \quad (6)$$

and

$$\mathbf{X}_2^T = \Big[ \underbrace{\mathbf{J}(\mathbf{R}_2^1) \ldots \mathbf{J}(\mathbf{R}_2^{N_2})}_{\text{Scatterer 2}} \Big]. \quad (7)$$

The source term $\mathbf{b}$ is defined as

$$\mathbf{b}^T = \left[ \mathbf{b}_1^T \ \mathbf{b}_2^T \right], \quad (8)$$

with

$$\mathbf{b}_1^T = \Big[ \underbrace{\hat{\mathbf{n}}_1 \times \mathbf{H}^i\left(\mathbf{R}_1^1\right) \ldots \hat{\mathbf{n}}_1 \times \mathbf{H}^i\left(\mathbf{R}_1^{N_1}\right)}_{\text{Scatterer 1}} \Big], \quad (9)$$

$$\mathbf{b}_2^T = \Big[ \underbrace{\hat{\mathbf{n}}_2 \times \mathbf{H}^i\left(\mathbf{R}_2^1\right) \ldots \hat{\mathbf{n}}_2 \times \mathbf{H}^i\left(\mathbf{R}_2^{N_2}\right)}_{\text{Scatterer 2}} \Big], \quad (10)$$

To solve the linear system, the matrix $\bar{\mathbf{Z}}$ is expressed from sub-matrices as

$$\bar{\mathbf{Z}} = \begin{bmatrix} \bar{\mathbf{Z}}_1 & \bar{\mathbf{Z}}_{21} \\ \bar{\mathbf{Z}}_{12} & \bar{\mathbf{Z}}_2 \end{bmatrix}. \quad (11)$$

$\bar{\mathbf{Z}}_1$ corresponds exactly to the impedance matrix of the first scatterer as if it is assumed to be alone (in free space), $\bar{\mathbf{Z}}_2$ corresponds to the impedance matrix of the second scatterer as if it is assumed to be alone (in free space). $\bar{\mathbf{Z}}_{21}$ and $\bar{\mathbf{Z}}_{12}$ can be interpreted as coupling matrices for the interaction between $S_1$ and $S_2$. The inverse of matrix $\bar{\mathbf{Z}}$ can be expressed as [4]

$$\bar{\mathbf{Z}}^{-1} = \begin{bmatrix} \bar{\mathbf{T}} & \bar{\mathbf{U}} \\ \bar{\mathbf{V}} & \bar{\mathbf{W}} \end{bmatrix}, \tag{12}$$

with

$$\begin{cases} \bar{\mathbf{T}} = \left(\bar{\mathbf{Z}}_1 - \bar{\mathbf{Z}}_{21}\bar{\mathbf{Z}}_2^{-1}\bar{\mathbf{Z}}_{12}\right)^{-1} \\ \bar{\mathbf{U}} = -\left(\bar{\mathbf{Z}}_1 - \bar{\mathbf{Z}}_{21}\bar{\mathbf{Z}}_2^{-1}\bar{\mathbf{Z}}_{12}\right)^{-1}\bar{\mathbf{Z}}_{21}\bar{\mathbf{Z}}_2^{-1} \\ \bar{\mathbf{V}} = -\bar{\mathbf{Z}}_2^{-1}\bar{\mathbf{Z}}_{12}\left(\bar{\mathbf{Z}}_1 - \bar{\mathbf{Z}}_{21}\bar{\mathbf{Z}}_2^{-1}\bar{\mathbf{Z}}_{12}\right)^{-1} \\ \bar{\mathbf{W}} = \bar{\mathbf{Z}}_2^{-1} + \bar{\mathbf{Z}}_2^{-1}\bar{\mathbf{Z}}_{12}\left(\bar{\mathbf{Z}}_1 - \bar{\mathbf{Z}}_{21}\bar{\mathbf{Z}}_2^{-1}\bar{\mathbf{Z}}_{12}\right)^{-1}\bar{\mathbf{Z}}_{21}\bar{\mathbf{Z}}_2^{-1} \end{cases}, \tag{13}$$

and the unknown vector $\mathbf{X}$ is obtained as

$$\begin{bmatrix} \mathbf{X}_1 \\ \mathbf{X}_2 \end{bmatrix} = \bar{\mathbf{Z}}^{-1}\begin{bmatrix} \mathbf{b}_1 \\ \mathbf{b}_2 \end{bmatrix} = \begin{bmatrix} \bar{\mathbf{T}}\mathbf{b}_1 + \bar{\mathbf{U}}\mathbf{b}_2 \\ \bar{\mathbf{V}}\mathbf{b}_1 + \bar{\mathbf{W}}\mathbf{b}_2 \end{bmatrix}. \tag{14}$$

By using Equations (13) and (14), the current on the upper scatterer $\mathbf{X}_1$ can be expressed as

$$\mathbf{X}_1 = \left(\bar{\mathbf{Z}}_1 - \bar{\mathbf{Z}}_{21}\bar{\mathbf{Z}}_2^{-1}\bar{\mathbf{Z}}_{12}\right)^{-1}\mathbf{b}_1 - \left(\bar{\mathbf{Z}}_1 - \bar{\mathbf{Z}}_{21}\bar{\mathbf{Z}}_2^{-1}\bar{\mathbf{Z}}_{12}\right)^{-1}\bar{\mathbf{Z}}_{21}\bar{\mathbf{Z}}_2^{-1}\mathbf{b}_2, \tag{15}$$

which leads to

$$\mathbf{X}_1 = \left(\bar{\mathbf{Z}}_1 - \bar{\mathbf{Z}}_{21}\bar{\mathbf{Z}}_2^{-1}\bar{\mathbf{Z}}_{12}\right)^{-1}\left(\mathbf{b}_1 - \bar{\mathbf{Z}}_{21}\bar{\mathbf{Z}}_2^{-1}\mathbf{b}_2\right) = \left(\bar{\mathbf{I}} - \bar{\mathbf{M}}_{c,1}\right)^{-1}\bar{\mathbf{Z}}_1^{-1}\left(\mathbf{b}_1 - \bar{\mathbf{Z}}_{21}\bar{\mathbf{Z}}_2^{-1}\mathbf{b}_2\right), \tag{16}$$

where $\bar{\mathbf{I}}$ is the identity matrix, and $\bar{\mathbf{M}}_{c,1}$ is a characteristic matrix expressed as

$$\bar{\mathbf{M}}_{c,1} = \bar{\mathbf{Z}}_1^{-1}\bar{\mathbf{Z}}_{21}\bar{\mathbf{Z}}_2^{-1}\bar{\mathbf{Z}}_{12}. \tag{17}$$

The first term in Equation (16) can be expanded as an infinite series over $p$

$$\left(\bar{\mathbf{I}} - \bar{\mathbf{M}}_{c,1}\right)^{-1} = \sum_{p=0}^{p=\infty}\bar{\mathbf{M}}_{c,1}^{p}. \tag{18}$$

For the numerical computation, the sum must be truncated at the order $P_{\text{E-PILE}}$. From Equations (17) and (18), the unknown current on the upper scatterer $\mathbf{X}_1$ is then expressed as

$$\mathbf{X}_1 = \left[\sum_{p=0}^{p=P_{\text{E-PILE}}}\bar{\mathbf{M}}_{c,1}^{p}\right]\bar{\mathbf{Z}}_1^{-1}\left(\mathbf{b}_1 - \bar{\mathbf{Z}}_{21}\bar{\mathbf{Z}}_2^{-1}\mathbf{b}_2\right) = \sum_{p=0}^{p=P_{\text{E-PILE}}}\bar{\mathbf{X}}_1^{(p)}, \tag{19}$$

in which

$$\begin{cases} \mathbf{X}_1^{(0)} = \bar{\mathbf{Z}}_1^{-1}\left(\mathbf{b}_1 - \bar{\mathbf{Z}}_{21}\bar{\mathbf{Z}}_2^{-1}\mathbf{b}_2\right) & \text{for } p = 0 \\ \mathbf{X}_1^{(p)} = \bar{\mathbf{M}}_{c,1}\bar{\mathbf{X}}_1^{(p-1)} & \text{for } p > 0 \end{cases}. \tag{20}$$

The unknown vector $\mathbf{X}_2$ is obtained by substituting in Equations (20), (19), and (17), subscripts $1, 2, 12, 21$ for subscripts $2, 1, 21, 12$, respectively.

The norm of the complex matrix $\left|\bar{\mathbf{M}}_{c,1}\right|$ is defined by its spectral radius, i.e., the modulus of its eigenvalue which has the highest modulus. Expansion (18) is then valid if $\left|\bar{\mathbf{M}}_{c,1}\right|$ is smaller than one. $\bar{\mathbf{M}}_{c,1}$ has a clear physical interpretation as shown in Figure 2: in the zeroth order terms, $\bar{\mathbf{Z}}_1^{-1}$ accounts for the local interactions on the upper scatterer, so $\mathbf{X}_1^{(0)}$ corresponds to the contribution of the scattering on the upper scatterer, when it is illuminated by the direct incident field ($\mathbf{b}_1$) and the direct scattered field by the lower scatterer ($-\bar{\mathbf{Z}}_{21}\bar{\mathbf{Z}}_2^{-1}\mathbf{b}_2$). In the first order term, $\mathbf{X}_1^{(1)} = \bar{\mathbf{M}}_{c,1}\mathbf{X}_1^{(0)}$, $\bar{\mathbf{Z}}_{12}$

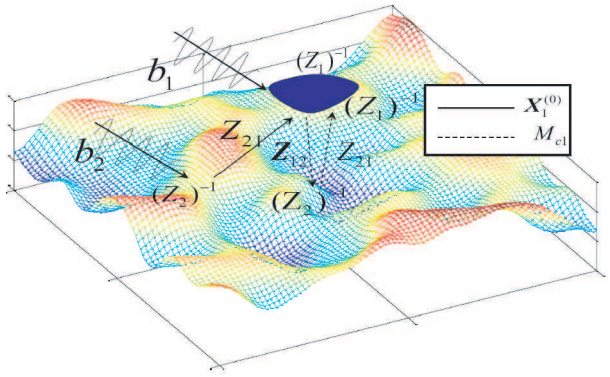


**Figure 2.** Physical interpretation of E-PILE method.

propagates the resulting upper field information, $\mathbf{X}_1^{(0)}$, toward the lower scatterer, $\bar{\mathbf{Z}}_2^{-1}$ accounts for the local interactions on this scatterer, and $\bar{\mathbf{Z}}_{21}$ re-propagates the resulting contribution toward the upper scatterer; finally, $\bar{\mathbf{Z}}_1^{-1}$ updates the field values on the upper scatterer. So the characteristic matrix $\bar{\mathbf{M}}_{c,1}$ realizes a back and forth between the upper scatterer and the lower one. The order $P_{\text{E-PILE}}$ of E-PILE, corresponds to the $P_{\text{E-PILE}}$ back and forth between the upper and the lower scatterer. In the same manner, $\bar{\mathbf{M}}_{c,2}$ realizes a back and forth between the lower scatterer and the upper one.

Once the equation $\bar{\mathbf{Z}}\mathbf{X} = \mathbf{b}$ is solved for $\mathbf{X}$, the scattered fields are computed by using Huygen's principle on the electric current densities, and the normalized Radar Cross Section (NRCS) of the two scatterers can be calculated by

$$\text{NRCS} = \lim_{R\to\infty} 4\pi R^2 \frac{\|\mathbf{E}^s\|^2}{2\eta P_i}, \tag{21}$$

in which $\mathbf{E}^s$ is the total scattered electric field in the far field region, and $P_i$ is the incident power calculated by

$$P_i = \frac{2\pi^2}{\eta} \int_{k_\rho<k} dk_x dk_y \left\|E_{TE}(k_x, k_y)\right\|^2 (kz/k). \tag{22}$$

The most complex operation in the calculation of $\mathbf{X}_1$ and $\mathbf{X}_2$ is $\bar{\mathbf{Z}}_1^{-1}$ and $\bar{\mathbf{Z}}_2^{-1}$. This calculation concerns the local interactions on both scatterer 1 and scatterer 2. One way to speed up this operation is to make a hybridization between the E-PILE method and the PO approximation.

## 3. HYBRIDIZATION OF E-PILE WITH PO APPROXIMATION

In the previous section, we have developed an exact numerical method E-PILE, based on the method of moments, to study the scattering from an object above a rough surface for a three-dimensional problem. The E-PILE is extremely powerful but it is limited to electrically small and moderately large electromagnetic structures, because its computation cost increases rapidly with an increase of the electrical size of the problem. Therefore, one strategy to reduce the computation time and memory requirements is to hybridize the E-PILE method with the PO approximation which is often used to approximate the current in the illuminated region of large, smooth, conducting bodies.

Let a PEC structure be excited by a time harmonic electromagnetic field of intensities $\mathbf{E}^i$ and $\mathbf{H}^i$. The distribution of surface electric currents on the structure can be evaluated using the PO approximation as follows

$$\mathbf{J}_{\text{PO}} = 2\hat{\mathbf{n}}(\mathbf{R}) \times \mathbf{H}^i(\mathbf{R}) \quad \forall \mathbf{R} \in S_i, \tag{23}$$

where $S_i$ is the illuminated surface.

Let us consider the 0th order of E-PILE

$$\mathbf{X}_1^{(0)} = \bar{\mathbf{Z}}_1^{-1} \left(\mathbf{b}_1 - \bar{\mathbf{Z}}_{21}\bar{\mathbf{Z}}_2^{-1}\mathbf{b}_2\right), \tag{24}$$

where $\mathbf{b}_1 = \hat{\mathbf{n}}_1(\mathbf{R}_1) \times \mathbf{H}^i(\mathbf{R}_1)$ and $\mathbf{b}_2 = \hat{\mathbf{n}}_2(\mathbf{R}_2) \times \mathbf{H}^i(\mathbf{R}_2)$ are the tangential incident fields on the first and second scatterer, respectively.

In Equation (24), one can split up the excitation into two sources: one due to the direct illumination of the incident field $\mathbf{b}_1$ and the other one due to the coupling interaction with the second scatterer $\bar{\mathbf{Z}}_{21}\bar{\mathbf{Z}}_2^{-1}\mathbf{b}_2$. The expression $\bar{\mathbf{Z}}_2^{-1}\mathbf{b}_2$ corresponds to the surface current density on the second scatterer as if it assumed to be in free space. By applying the PO approximation, the diagonal elements of $\bar{\mathbf{Z}}_2^{-1}$ are equal to 2 on the illuminated region of the surface and 0 otherwise (no point to point interaction with PO). The expression $\bar{\mathbf{Z}}_1^{-1}\mathbf{b}_1$ corresponds to the surface current density on the first scatterer as if it assumed to be in free space. By applying the PO approximation, the diagonal elements of $\bar{\mathbf{Z}}_1^{-1}$ are equal to 2 on the illuminated region of the surface and 0 otherwise. As a result, $\bar{\mathbf{Z}}_1^{-1}$ and $\bar{\mathbf{Z}}_2^{-1}$ are not calculated, consequently the calculation of E-PILE method will be strongly accelerated.

Mathematically, applying the PO approximation on the two scatterers for the case of a plate above a rough surface can be explained as follows:

**PO on the first scatterer (PO1)**: First, the illuminated and shadowed regions must be defined to apply the PO approximation. As illustrated in Figure 3, the top side of the plate $S_{\text{top}}$ is illuminated by the incident field $\mathbf{b}_1$, while the bottom side $S_{\text{bottom}}$ is illuminated by the scattered field from the rough surface $\bar{\mathbf{Z}}_{21}\bar{\mathbf{Z}}_2^{-1}\mathbf{b}_2$. So $\mathbf{b}_1$ should be modified as follows:

$$\mathbf{b}_1' = \begin{bmatrix} \mathbf{b}_1^{\text{top}} \\ \mathbf{b}_1^{\text{bottom}} \end{bmatrix}, \tag{25}$$

where

$$\mathbf{b}_1^{\text{top}} = \begin{bmatrix} \hat{\mathbf{n}} \times \mathbf{H}^i(\mathbf{R}_1^1) \\ \vdots \\ \hat{\mathbf{n}} \times \mathbf{H}^i(\mathbf{R}_1^{N_{\text{top}}}) \end{bmatrix}, \tag{26}$$

is the incident field on the top side and

$$\mathbf{b}_1^{\text{bottom}} = \left.\begin{bmatrix} 0 \\ \vdots \\ 0 \end{bmatrix}\right\} N_{\text{bottom}}, \tag{27}$$

is the incident field on the bottom side. $N_{\text{top}}$ and $N_{\text{bottom}}$ are the number of sampling points on the top and bottom side, respectively.

The coupling matrix $\bar{\mathbf{Z}}_{21}$ should also be modified as:

$$\bar{\mathbf{Z}}_{21}' = \begin{bmatrix} \bar{\mathbf{Z}}_{21}^{\text{top}} \\ \bar{\mathbf{Z}}_{21}^{\text{bottom}} \end{bmatrix}, \tag{28}$$

where $\bar{\mathbf{Z}}_{21}^{\text{top}}$ is the coupling matrix between the rough surface and the top side of the plate. Since PO approximation is used, $\bar{\mathbf{Z}}_{21}^{\text{top}}$ is a zero filled matrix because the scattered field from the rough surface illuminates only the bottom side of the plate. $\bar{\mathbf{Z}}_{21}^{\text{bottom}}$ is the coupling matrix between the rough surface and the bottom side of the plate which is illuminated by the scattered field from the rough surface.

As a result Equation (20) in the E-PILE algorithm is simplified as:

$$\begin{cases} \mathbf{X}_1^{(0)} = 2\left(\mathbf{b}_1' - \bar{\mathbf{Z}}_{21}' 2\mathbf{b}_2\right) & \text{for } p = 0 \\ \mathbf{X}_1^{(p)} = \bar{\mathbf{M}}_{c,1}' \bar{\mathbf{X}}_1^{(p-1)} & \text{for } p > 0 \end{cases}. \tag{29}$$

in which $\bar{\mathbf{M}}_{c,1}' = 2\bar{\mathbf{Z}}_{21}' 2\bar{\mathbf{Z}}_{12}$.

**PO on the second scatterer (PO2)**: As illustrated in Figure 4, the rough surface is illuminated by the direct incident field $\mathbf{b}_2$, and the scattered field from the plate $\bar{\mathbf{Z}}_{12}\bar{\mathbf{Z}}_1^{-1}\mathbf{b}_1'$. These two fields illuminate the same side of the rough surface.

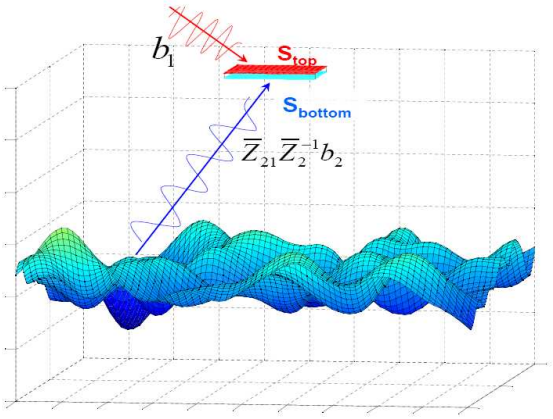


**Figure 3.** Illustration of propagation paths according to PO1.

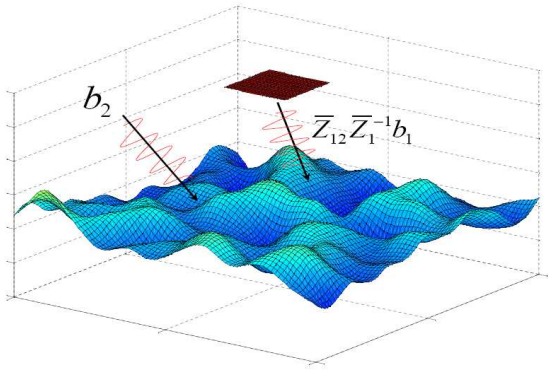


**Figure 4.** Illustration of propagation paths according to PO2.

The unknown currents on the rough surface can be calculated from the E-PILE algorithm as follows:

$$\begin{cases} \mathbf{X}_2^{(0)} = 2\left(\mathbf{b}_2 - \bar{\mathbf{Z}}_{12}2\mathbf{b}_1'\right) & \text{for } p = 0 \\ \mathbf{X}_2^{(p)} = \bar{\mathbf{M}}_{c,2}'\bar{\mathbf{X}}_2^{(p-1)} & \text{for } p > 0 \end{cases}. \tag{30}$$

in which $\bar{\mathbf{M}}_{c,2}' = 2\bar{\mathbf{Z}}_{12}2\bar{\mathbf{Z}}_{21}'$.

In conclusion, the inverse of the impedance matrices $\bar{\mathbf{Z}}_1^{-1}$ and $\bar{\mathbf{Z}}_2^{-1}$ are not calculated. Thus, the complexity for the inversion $\mathcal{O}(N_1^3)$ becomes 1 and $\mathcal{O}(N_2^3) \to 1$ also. So the workload is reduced as the expense of reduced accuracy. PO1 and PO2 shadowing effects being geometrically taken into account in the incident vector and during the coupling matrix fillings. Indeed, we can note that the E-PILE combined with the PO on both scatterers is similar to the Iterative Physical Optics (IPO) [20].

## 4. NUMERICAL RESULTS

### 4.1. Validity of E-PILE Method

The E-PILE method is tested firstly for the case of two parallel horizontal PEC plates, and secondly for the case of a PEC plate above a PEC randomly rough surface. To quantify the convergence of the E-PILE method versus its order, the Relative Residual Error ($r_e$) is introduced and defined as

$$r_e = \frac{\text{norm}(\mathbf{X} - \mathbf{X}_{\text{LU}})}{\text{norm}(\mathbf{X}_{\text{LU}})}. \tag{31}$$

$\mathbf{X}$ represents the electric current induced on the surface. The subscript LU means that the vector is computed from LU inversion. For a low $r_e$, the vector $\mathbf{X}$ obtained from the E-PILE method is close to $\mathbf{X}_{\text{LU}}$ computed from the direct LU inversion. We compare the results obtained by E-PILE with those computed from the MoM with a direct LU inversion (MoM-LU), which is the reference method here.

Consider two parallel plates shown in Figure 5, the dimensions of the upper plate are $S_1 = 2\lambda_0 \times 2\lambda_0$, the dimensions of the lower one are $S_2 = 6\lambda_0 \times 6\lambda_0$, the distance $D$ between the two plates is $5\lambda_0$, sampling steps are $\Delta x = \Delta y = \lambda_0/8$. An incident EM plane wave vertically polarized illuminates the system, with angles $\theta_i = 0°$ for results in Figure 6(a) and $\theta_i = 45°$ for results in Figure 6(b), where the Radar Cross Section (RCS) computed from the E-PILE method is compared with that obtained from MoM-LU versus the scattering angle $\theta_s$.

Figure 6 shows that as the order of E-PILE increases it converges to LU (E-PILE 8 is closer to LU than E-PILE 0). Other simulations, not depicted here, showed that the E-PILE method converges more quickly as the distance between the two plates increases, since the electromagnetic coupling is less important than the previous case. In fact, the order $P_{\text{E-PILE}}$ is directly related to the coupling between the two scatterers.

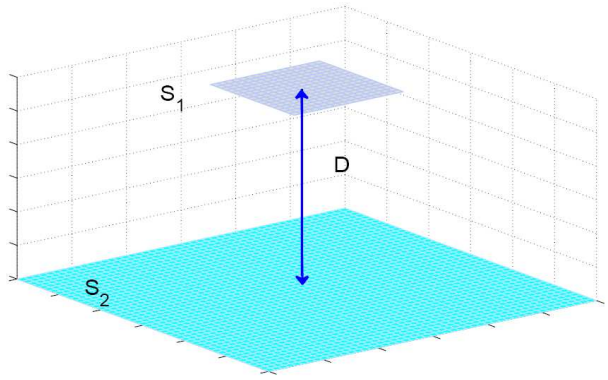


**Figure 5.** Composite model of two parallel horizontal PEC plates.

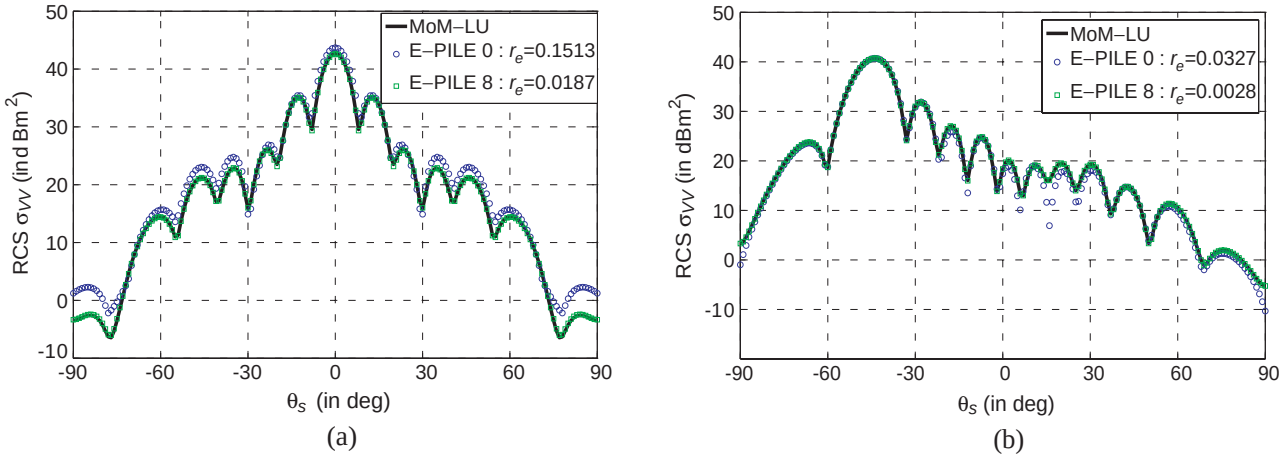


**Figure 6.** Convergence of E-PILE versus its order, for the case of two parallel plates, $S_1 = 2\lambda_0 \times 2\lambda_0$, $S_2 = 6\lambda_0 \times 6\lambda_0$, $D = 5\lambda_0$: (a) $\theta_i = 0°$, (b) $\theta_i = 45°$.

Let us now consider the configuration of a PEC plate above a PEC rough surface as shown in Figure 7. The dimensions of the plate are $S_1 = 2\lambda_0 \times 2\lambda_0$ and the rough surface obeys a Gaussian process with a Gaussian height spectrum with root mean square height $\sigma_z = 0.2\lambda_0$, correlation lengths are $L_{cx} = L_{cy} = 1\lambda_0$. The dimensions of the rough surface are $S_2 = 6\lambda_0 \times 6\lambda_0$, the distance $D$ between the plate and the rough surface is $5\lambda_0$, sampling steps are $\Delta_x = \Delta_y = \lambda_0/8$. An incident EM plane wave vertically polarized illuminates the system, with angles $\theta_i = 0°$ for results in Figure 8(a) and $\theta_i = 45°$ for results in Figure 8(b), where the RCS computed from the E-PILE method is compared with that obtained from MoM-LU versus the scattering angle $\theta_s$.

Figure 8 shows that E-PILE method is also valid for this configuration, and as the order of E-PILE increases it converges to LU.

Now we focus on the convergence rate of the E-PILE method for the four previous scenarios:

(1) Scenario of Figure 6(a).
(2) Scenario of Figure 6(b).
(3) Scenario of Figure 8(a).
(4) Scenario of Figure 8(b).

Figure 9 compares the Relative Residual Error for each scenario versus E-PILE order. As a general remark, it can be observed that E-PILE converges more slowly for scenario (1). This is due to the value of the incidence angle $\theta_i = 0°$. Indeed, for this scenario more iterations (reflections between the two plates) are needed to obtain a weak field region on the lower plate as a result of the presence of the

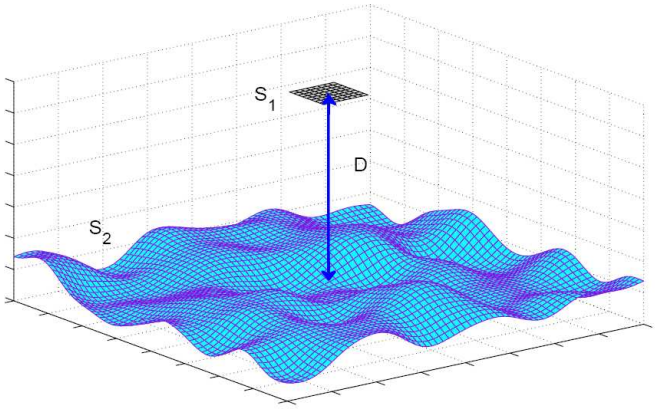


**Figure 7.** Composite model of a PEC plate above a PEC rough surface.

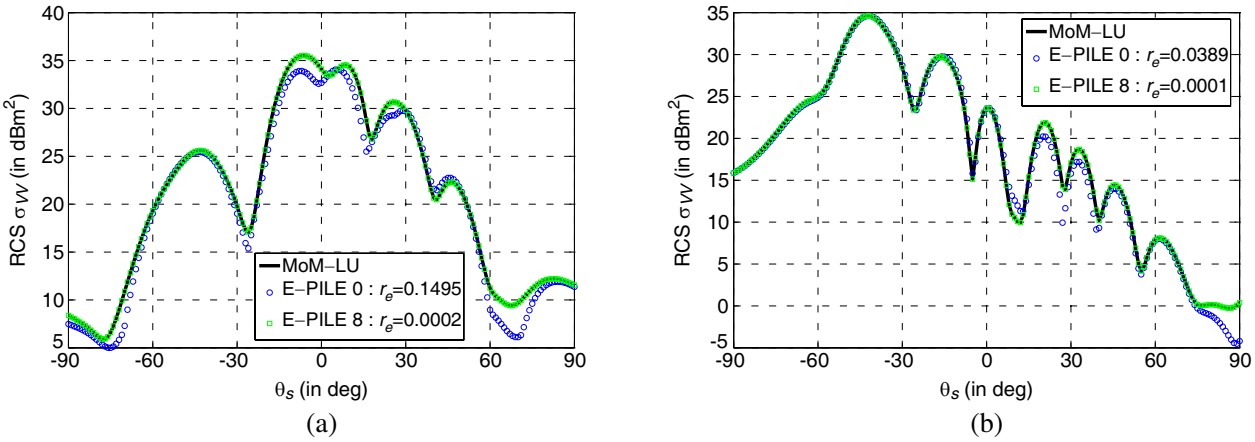


**Figure 8.** Convergence of E-PILE versus its order, for the case of a plate above a rough surface, $S_1 = 2\lambda_0 \times 2\lambda_0$, $S_2 = 6\lambda_0 \times 6\lambda_0$, $D = 5\lambda_0$, $\sigma_z = 0.2\lambda_0$, $L_{cx} = L_{cy} = 1\lambda_0$: (a) $\theta_i = 0°$, (b) $\theta_i = 45°$.

upper plate above it. Furthermore, If we choose $r_e = 0.02$ as a threshold value, then we can notice from Figure 9 that E-PILE converges more rapidly for scenarios (2) and (4) where $\theta_i = 45°$ than scenarios (1) and (3) where $\theta_i = 0°$. So we can conclude that E-PILE method is sensitive to the incidence angle.

### 4.2. Validity of E-PILE Hybridized with Physical Optics (E-PILE+PO1+PO2)

To validate our hybrid method E-PILE+PO1+PO2, comparisons with MoM-LU for two different configurations are proposed. The first one is the case of two parallel horizontal PEC plates, and the second one is the case of a PEC plate above a PEC rough surface, the order of E-PILE, $P_{\text{E-PILE}} = 8$, for all simulations.

Let us firstly consider the case of two parallel horizontal plates of dimensions $S_1 = 1\lambda_0 \times 1\lambda_0$, $S_2 = 8\lambda_0 \times 8\lambda_0$, the distance between them is $5\lambda_0$, and the sampling steps are $\Delta_x = \Delta_y = \lambda_0/8$. The two plates are illuminated by an EM plane wave with incidence angle of $\theta_i = 0°$. Comparisons of RCS versus $\theta_s$ are shown in Figures 10(a) and 10(b). From the Figures, a very good agreement is observed between the hybrid method E-PILE+PO1+PO2 and MoM-LU, for both $VV$ and $HH$ polarizations.

Figure 11 shows the current distribution obtained by E-PILE+PO1+PO2, on both plates for the previous configuration with $VV$ polarization. The field scattered from $S_2$ illuminates only the bottom side of $S_1$, whereas the incident wave illuminates the upper side of $S_1$. Consequently, currents are constant on $S_{1\text{top}}$ and the coupling mechanism between $S_1$ and $S_2$ implies a non-null current on $S_{1\text{bottom}}$. We can also notice that the presence of $S_1$ above $S_2$, creates a shadowing region (dark region with less

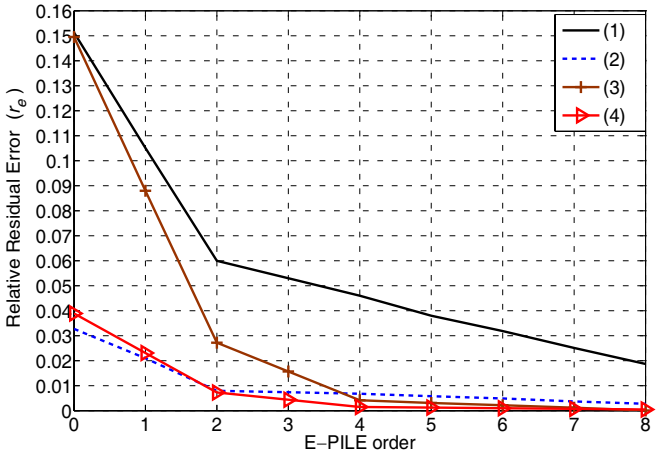


**Figure 9.** Relative residual error versus E-PILE order.

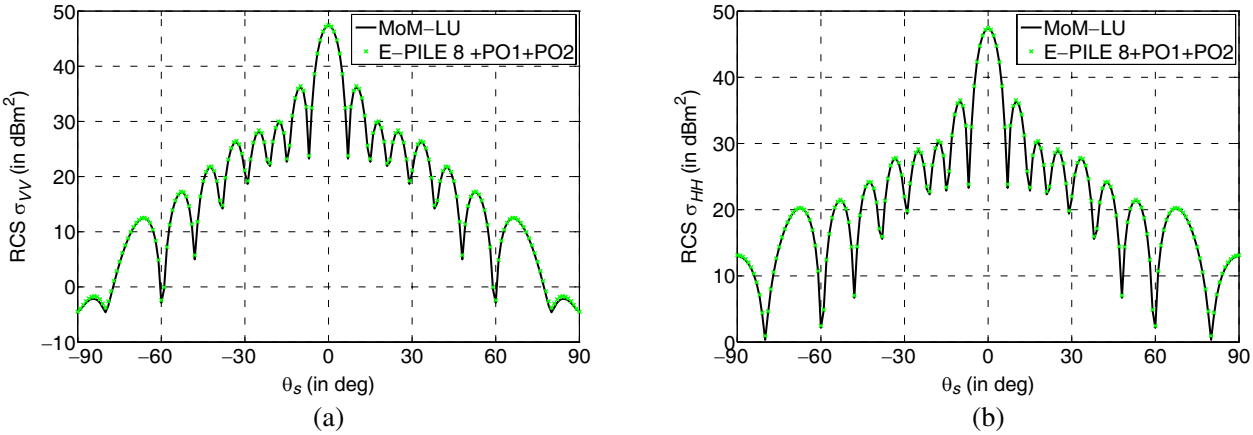


**Figure 10.** Comparison of the radar cross-section of two parallel plates computed from the hybrid method (EPILE 8+PO1+PO2) with that obtained from the reference method (MoM-LU) versus the scattering angle. The parameters are $S_1 = 1\lambda_0 \times 1\lambda_0$, $S_2 = 8\lambda_0 \times 8\lambda_0$, $D = 5\lambda_0$, $\theta_i = 0°$: (a) vertical polarization, (b) horizontal polarization.

current) on the lower surface $S_2$. As a result, it seems that our method explains well the expected physical phenomena.

As a second example, consider the case of a plate of dimensions $S_1 = 1\lambda_0 \times 1\lambda_0$ above a rough surface which obeys a Gaussian process with $\sigma_z = 0.2\lambda_0$, $L_{cx} = L_{cy} = 1\lambda_0$, the dimensions of the rough surface are $8\lambda_0 \times 8\lambda_0$, the distance $D$ between the plate and the rough surface is $5\lambda_0$, sampling steps are $\Delta_x = \Delta_y = \lambda_0/8$. The incident plane wave has an incidence angle of $\theta_i = 0°$. Comparisons of RCS are shown in Figures 12(a) and 12(b).

In our hybrid method, PO is applied on both the plate and rough surface. It is shown in [18, 19] that multiple reflections phenomena on the rough surface is very weak and can be neglected for surfaces of root mean square slope less than 0.35 ($\sigma_s < 0.35$). In our case $\sigma_s = \frac{\sqrt{2}\sigma_z}{Lc} \approx 0.28$. Figures 12(a) and 12(b) show that the hybrid method works well for the backscattering from about $\theta_s = -50°$ to $\theta_s = +50°$. The disagreement observed at grazing angles is due to the edge diffraction. Thus, in order to avoid this limitation an incident tapered wave is applied to the system for larger problems.

Hereafter we investigate the previous cases but for larger electromagnetic problems. Consider the configuration of two parallel horizontal plates of dimensions $S_1 = 2\lambda_0 \times 2\lambda_0$, $S_2 = 14\lambda_0 \times 14\lambda_0$. We use an incident tapered wave with $\theta_i = 0°$, $g = L/2$ ($L$ is $L_x$ or $L_y$). Comparisons of RCS versus $\theta_s$ are

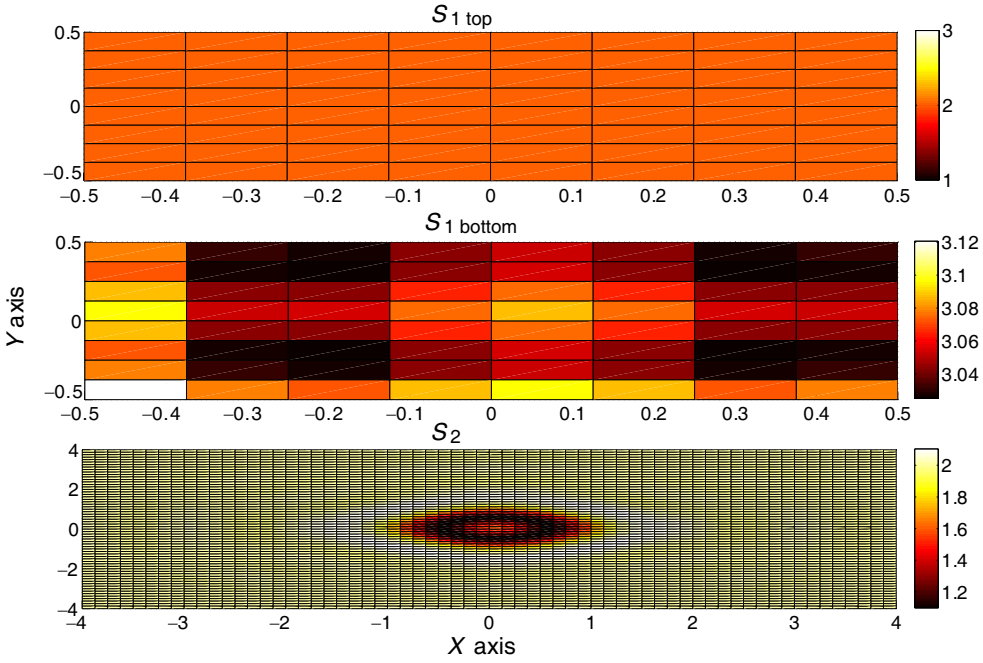


**Figure 11.** Current distribution on the two plates computed from the hybrid method.

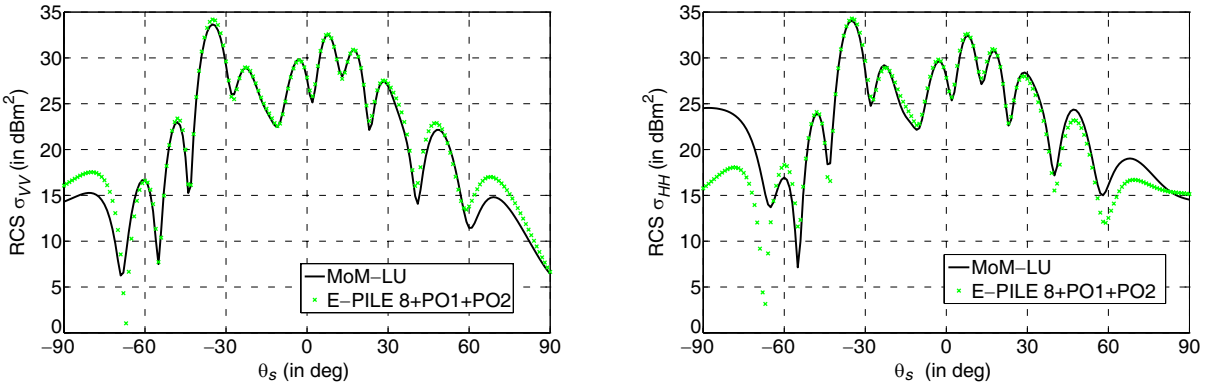


(a) (b)

**Figure 12.** Comparison of the radar cross-section of a plate above a rough surface computed from the hybrid method (EPILE 8+PO1+PO2) with that obtained from the reference method (MoM-LU) versus the scattering angle. The parameters are $S_1 = 1\lambda_0 \times 1\lambda_0$, $S_2 = 8\lambda_0 \times 8\lambda_0$, $D = 5\lambda_0$, $\sigma_z = 0.2\lambda_0$, $L_{cx} = L_{cy} = 1\lambda_0$, $\theta_i = 0°$: (a) vertical polarization, (b) horizontal polarization.

shown in Figures 13(a) and 13(b). From these figures, a very good agreement is observed between the hybrid method E-PILE+PO1+PO2 and MoM-LU, for both $VV$ and $HH$ polarizations.

Now let us consider the case of a plate of dimensions $S_1 = 2\lambda_0 \times 2\lambda_0$ above a rough surface which obeys a Gaussian process with $\sigma_z = 0.2\lambda_0$, $L_{cx} = L_{cy} = 1\lambda_0$, the dimensions of the rough surface are $14\lambda_0 \times 14\lambda_0$, the distance $D$ between the plate and the rough surface is $5\lambda_0$, sampling steps are $\Delta_x = \Delta_y = \lambda_0/8$. The incident tapered wave has an incidence angle of $\theta_i = 0°$ and $g = L/2$. Comparisons of RCS are shown in Figures 14(a) and 14(b).

Figures 14(a) and 14(b) show a good agreement between the hybrid and the reference method for all scattering angles in the two polarizations $VV$ and $HH$. We can conclude that using the tapered wave allows us to reduce the inaccuracies in the results shown in Figures 14(a) and 14(b).

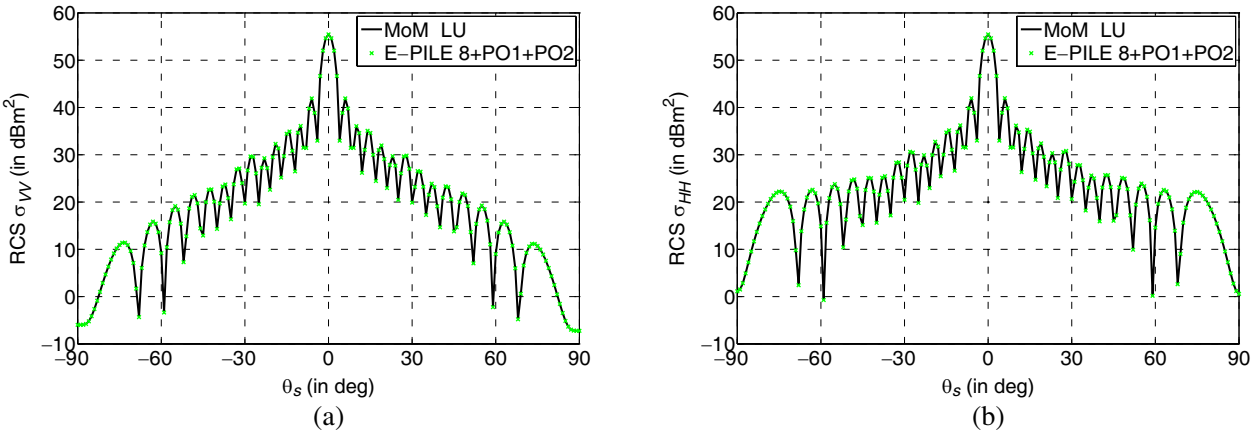


**Figure 13.** Comparison of the radar cross-section of two parallel plates computed from the hybrid method (EPILE 8+PO1+PO2) with that obtained from the reference method (MoM-LU) versus the scattering angle. The parameters are $S_1 = 2\lambda_0 \times 2\lambda_0$, $S_2 = 14\lambda_0 \times 14\lambda_0$, $D = 5\lambda_0$, $\theta_i = 0°$: (a) vertical polarization, (b) horizontal polarization.

### 4.3. Convergence of E-PILE

The purpose of this subsection is to study the influence of the parameters of the system on the convergence of the E-PILE method. In order to obtain the order $P_{\text{E-PILE}}$ which permits us to have a good convergence, the Relative Residual Error ($r_e$) must be smaller than a chosen value equal to $10^{-2}$ in what follows. We study hereafter the case of two parallel PEC plates.

#### *4.3.1. Influence of the Dimensions of the Plates*

Let us consider the problem of two parallel PEC plates, the lower plate dimensions are $6\lambda_0 \times 6\lambda_0$, while the upper plate length is not constant, the incident wave is vertically polarized with angle $\theta_i = 30°$, and the distance $D$ between the plates is $10\lambda_0$. Table 1 presents the order $P_{\text{E-PILE}}$ for each dimension of the upper plate.

From Table 1, we can notice that as the length of the upper plate increases, the order $P_{\text{E-PILE}}$

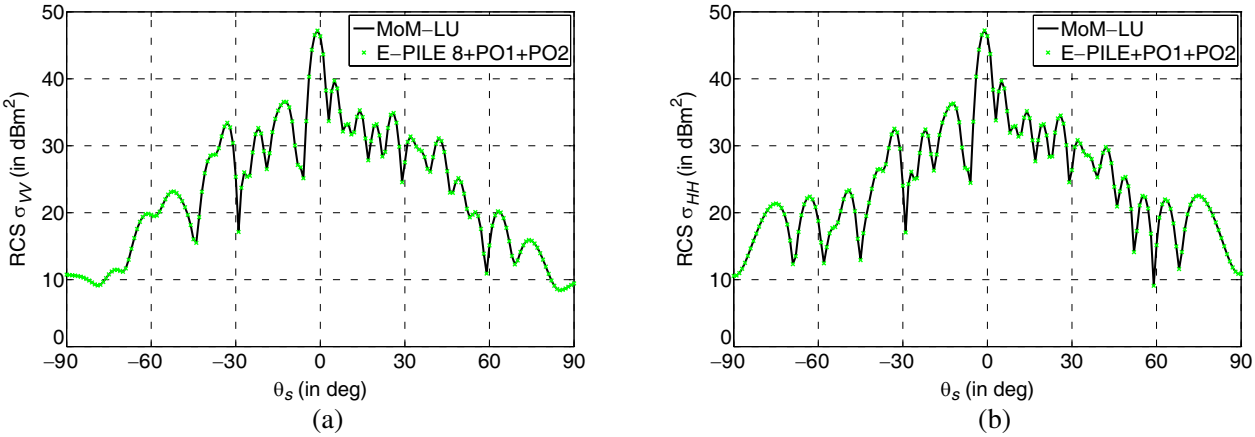


**Figure 14.** Comparison of the radar cross-section of a plate above a rough surface computed from the hybrid method (EPILE 8+PO1+PO2) with that obtained from the reference method (MoM-LU) versus the scattering angle. The parameters are $S_1 = 2\lambda_0 \times 2\lambda_0$, $S_2 = 14\lambda_0 \times 14\lambda_0$, $D = 5\lambda_0$, $\sigma_z = 0.2\lambda_0$, $L_{cx} = L_{cy} = 1\lambda_0$, $\theta_i = 0°$: (a) vertical polarization, (b) horizontal polarization.

**Table 1.** Order $P_{\text{E-PILE}}$ versus the dimensions of the upper plate $S_1$. The parameters are $S_2 = 6\lambda_0 \times 6\lambda_0$, $\theta_i = 30°$, $D = 10\lambda_0$.

| Upper plate dimensions | $P_{\text{E-PILE}}$ |
|---|---|
| $S_1 = 1\lambda_0 \times 1\lambda_0$ | 1 |
| $S_1 = 2\lambda_0 \times 2\lambda_0$ | 3 |
| $S_1 = 4\lambda_0 \times 4\lambda_0$ | 10 |

increases, which means that we have more forth and back between the lower and the upper plate. Indeed, as the dimensions of the upper plate increase and become closer to the dimensions of the lower one, the region between the two plates can be described as an open wave guide, so the wave is guided between the two plates and induces more reflections.

*4.3.2. Influence of the Distance between the Two Plates*

The same configuration of two parallel PEC plates is tested here, $S_1 = 2\lambda_0 \times 2\lambda_0$, $S_2 = 6\lambda_0 \times 6\lambda_0$, the distance $D$ between the two plates is not constant, the incident wave is vertically polarized with angle $\theta_i = 30°$. Table 2 presents the order $P_{\text{E-PILE}}$ for each distance between the two plates.

**Table 2.** Order $P_{\text{E-PILE}}$ versus the distance $D$ between the two plates. The parameters are $S_1 = 2\lambda_0 \times 2\lambda_0$, $S_2 = 6\lambda_0 \times 6\lambda_0$, $\theta_i = 30°$.

| The distance $D$ | $P_{\text{E-PILE}}$ |
|---|---|
| $D = 3\lambda_0$ | 8 |
| $D = 10\lambda_0$ | 3 |
| $D = 15\lambda_0$ | 1 |

Table 2 shows that as the distance between the two plates decreases, the order $P_{\text{E-PILE}}$ increases, as a consequence of higher coupling between the two plates, this implies that the E-PILE method converges more quickly for a larger distance between the two plates.

*4.3.3. Influence of Lower Surface Roughness*

Let us consider the case of a PEC plate of dimensions $S_1 = 2\lambda_0 \times 2\lambda_0$ above a PEC rough surface of dimensions $S_2 = 6\lambda_0 \times 6\lambda_0$ which obeys a Gaussian process, with $L_{cx} = L_{cy} = 1\lambda_0$, but $\sigma_z$ is not constant as in Table 3. The distance $D$ between the two scatterers is $5\lambda_0$, and the incident wave is vertically polarized with angle $\theta_i = 30°$. Table 3 presents the order $P_{\text{E-PILE}}$ for each $\sigma_z$ of the lower scatterer $S_2$.

**Table 3.** Order $P_{\text{E-PILE}}$ versus the lower surface mean square height. The parameters are $S_1 = 2\lambda_0 \times 2\lambda_0$, $S_2 = 6\lambda_0 \times 6\lambda_0$, $\theta_i = 30°$, $D = 5\lambda_0$.

| Mean square height | $P_{\text{E-PILE}}$ |
|---|---|
| $\sigma_z = 0\lambda_0$ | 4 |
| $\sigma_z = 0.2\lambda_0$ | 5 |
| $\sigma_z = 0.5\lambda_0$ | 7 |

Table 3 shows that as $\sigma_z$ of the lower surface increases, the order $P_{\text{E-PILE}}$ increases, which means that the surface roughness affects the order of E-PILE method.

### 4.4. Complexity

The complexity of the two algorithms (E-PILE) and (E-PILE+PO1+PO2) are given in Table 4, in which

- $T_1$ is the complexity of the matrix inversion for the local interactions on scatterer 1.
- $T_2$ is the complexity of the matrix inversion for the local interactions on scatterer 2.
- $T_{11}$ is the complexity of the matrix-vector product for the local interactions on scatterer 1.
- $T_{22}$ is the complexity of the matrix-vector product for the local interactions on scatterer 2.
- $T_{12}$ is the complexity of the matrix-vector product for a coupling step (object toward surface).
- $T_{21}$ is the complexity of the matrix-vector product for a coupling step (surface toward object).

**Table 4.** Complexity of E-PILE and E-PILE+PO1+PO2.

| Algorithm | $T_1$ | $T_{11}$ | $T_2$ | $T_{22}$ | $T_{12}$ | $T_{21}$ |
|---|---|---|---|---|---|---|
| E-PILE | $N_1^3$ | $N_1^2$ | $N_2^3$ | $N_2^2$ | $N_1N_2$ | $N_1N_2$ |
| E-PILE+PO1+PO2 | 0 | 1 | 0 | 1 | $N_1N_2$ | $N_1N_2/2$ |

To compare the computing time of the two algorithms (MoM-LU) and (E-PILE+PO1+PO2) which is closely related to the complexity, the case of two parallel plates $S_1$ above $S_2$ is considered, $S_2$ of dimensions $7\lambda_0 \times 7\lambda_0$, the length of $S_1$ is not constant. Comparisons of computing time versus the length of $S_1$ are shown in Figure 15. The CPU used is Intel(R) Xeon(R) 2.83 GHz with 16 GBytes of RAM. From Figure 15, we can notice that the hybrid method allows us to reduce greatly the computing time.

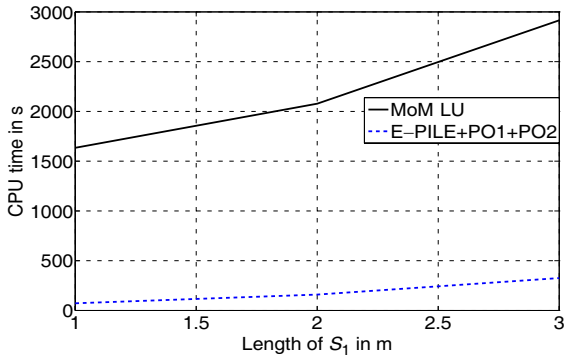


**Figure 15.** Comparison of computing time of the hybrid and rigorous method versus the length of $S_1$ for the case of two parallel plates $S_1$ above $S_2$.

One can evaluate the theoretical storage requirements by considering the plate above a rough surface for three methods: the MoM (with direct LU inversion of the impedance matrix of the whole scene), the E-PILE and the E-PILE+PO1+PO2. The MoM needs to store $(N_1 + N_2)^2$ complex elements. The memory requirements of E-PILE, E-PILE+PO1+PO2 are listed in Table 5.

From the table, one can see that the E-PILE method combined with the PO approximation permits us to significantly reduce the storage requirements.

**Table 5.** Storage requirements of E-PILE and E-PILE+PO1+PO2.

| Algorithm | $\bar{Z}_1$ | $\bar{Z}_{12}$ | $\bar{Z}_{21}$ | $\bar{Z}_2$ |
|---|---|---|---|---|
| E-PILE | $N_1^2$ | $N_1N_2$ | $N_1N_2$ | $N_2^2$ |
| E-PILE+PO1+PO2 | 1 | $N_1N_2$ | $\frac{N_1N_2}{2}$ | 1 |

## 5. CONCLUSION

In this paper, a new efficient hybrid method to study the electromagnetic scattering from a 3-D problem of two scatterers is presented. The method is based on the rigorous E-PILE method, originally developed to predict the field scattering from an object above a one-dimensional rough surface. In this work, the E-PILE method is extended to solve 3-D electromagnetic problems. Indeed, the E-PILE order is linked to the number of reflections between the two scatterers (object+rough surface). A major advantage of the E-PILE method is that it can be combined with algorithms originally developed to solve problems of scattering from a single scatterer in free space. Consequently, we combined the E-PILE method with the PO approximation to calculate the local interactions on the two scatterers. By this way there is no need to calculate the inverse of the impedance matrix for both scatterers, which will allow us to reduce the complexity of the E-PILE method. The hybrid method E-PILE+PO1+PO2 has then the complexity of $\mathcal{O}(N_1 N_2)$ instead of $\mathcal{O}((N_1 + N_2)^3)$ for MoM-LU where $N_1$ and $N_2$ are the number of sampling points on the object and rough surface, respectively. As a prospect of this paper, it could be interesting to use the FBSA approach to accelerate the calculation of the local interactions on the rough surface instead of using the PO approximation, as done in [5] for a 2-D problem.

## REFERENCES

1. Guo, L.-X., A.-Q. Wang, and J. Ma, "Study on EM scattering from 2-D target above 1-D large scale rough surface with low grazing incidence by parallel MoM based on PC clusters," *Progress In Electromagnetics Research*, Vol. 89, No. 5, 149–166, 2009.
2. Liu, P. and Y. Q. Jin, "The finite-element method with domain decomposition from electromagnetic bistatic scattering from the comprehensive model of a ship on and a target above a large scale rough sea surface," *IEEE Transactions on Geoscience and Remote Sensing*, Vol. 42, No. 5, 950–956, 2004.
3. Ye, H. and Y.-Q. Jin, "A hybrid analytical-numerical algorithm of scattering from an object above a rough surface," *IEEE Transactions on Geoscience and Remote Sensing*, Vol. 45, No. 5, 1174–1180, 2007.
4. Déchamps, N., N. De Beaucoudrey, C. Bourlier, and S. Toutain, "Fast numerical method for electromagnetic scattering by rough layered interfaces: Propagation-inside-layer expansion method," *Journal of the Optical Society of America A*, Vol. 23, 359–369, 2006.
5. Kubické, G., C. Bourlier, and J. Saillard, "Scattering by an object above a randomly rough surface from a fast numerical method: Extended PILE method combined with FB-SA," *Waves in Random and Complex Media*, Vol. 18, No. 3, 495–519, 2008.
6. Pino, M. R., F. Obelleiro, L. Landesa, and R. Burkholder, "Application of the fast mutipole method to the generalized forward-backward iterative algorithm," *Microwave and Optical Technology Letters*, Vol. 26, No. 2, 78–83, 2000.
7. Kubické, G. and C. Bourlier, "A fast hybrid method for scattering from a large object with dihedral effects above a large rough surface," *IEEE Transactions on Antennas and Wave Propagation*, Vol. 59, No. 1, 189–198, 2011.
8. Pino, M. R., L. Landesa, J. L. Rodriguez, F. Obelleiro, and R. Burkholder, "The generalized forward-backward method for analyzing the scattering from targets on ocean-like rough surfaces," *IEEE Transactions on Antennas and Wave Propagation*, Vol. 47, No. 5, 961–969, 1999.
9. Ye, H. and Y.-Q. Jin, "Fast iterative approach to difference electromagnetic scattering from the target above a rough surface," *IEEE Transactions on Geoscience and Remote Sensing*, Vol. 44, 108–115, 2006.
10. Ye, H. and Y.-Q. Jin, "FA hybrid KA-MoM algorithm for computation of scattering from a 3-D PEC target above a dielectric rough surface," *Radio Science*, Vol. 43, RS3005, 2008.
11. Guan, B., J. Zhang, X. Zhou, and T. Cui, "Electromagnetic scattering from objects above a rough surface using the method of moments with half-space green's function," *IEEE Transactions on Geoscience and Remote Sensing*, Vol. 47, No. 10, 3399–3405, 2009.
12. Johnson, J. T., "A Numerical study of scattering from an object above a rough surface," *IEEE Transactions on Antennas and Wave Propagation*, Vol. 50, No. 10, 1361–1367, 2002.

13. Johnson, J. T. and R. J. Burkholder, "Coupled canonical grid/discrete dipole approach for computing scattering from objects above or below a rough interface," *IEEE Transactions on Geoscience and Remote Sensing*, Vol. 39, No. 6, 1214–1220, 2001.
14. Johnson, J. T., "A study of the four-path model for scattering from an object above a half space," *Microwave and Optical Technology Letters*, Vol. 30, No. 6, 130–134, 2001.
15. Guo, L.-X., J. Li, and H. Zeng, "Bistatic scattering from a three-dimensional object above a two-dimensional randomly rough surface modeled with the parallel FDTD approach," *Journal of the Optical Society of America A*, Vol. 26, No. 11, 2383–2391, 2009.
16. Kuang, L. and Y.-Q. Jin, "Bistatic scattering from a three-dimensional object over a randomly rough surface using the FDTD algorithm," *IEEE Transactions on Antennas and Wave Propagation*, Vol. 55, No. 8, 2302–2312, 2007.
17. Kouali, M., G. Kubické, and C. Bourlier, "Extended propagation-inside-layer expansion method combined with the forward-backward method to study the scattering from an object above a rough surface," *Optics Letters*, Vol. 37, No. 14, 2985–2987, 2012.
18. Thorsos, E., "The validity of the Kirchhoff approximation for rough surface scattering using a Gaussian roughness spectrum," *Journal of the Acoustical Society of America*, Vol. 83, 87–92, 1988.
19. Bourlier, C., G. Berginc, and J. Saillard, "Monostatic and bistatic shadowing functions from a one-dimensional stationary randomly rough surface according to the observation length: I. Single scattering," *Waves in Random and Complex Media*, Vol. 12, No. 2, 145–174, 2002.
20. Obelleiro-Basteiro, F., J. Rodriguez, and R. Burkholder, "An iterative physical optics approach for analyzing the electromagnetic scattering by large open-ended cavities," *IEEE Transactions on Antennas and Wave Propagation*, Vol. 43, No. 4, 356–361, 1995.